

---

# Hypothesis Testing for Unknown Dynamical Systems and System Anomaly Detection via Autoencoders

---

**Haowei He**<sup>\*,†</sup>

hhw19@mails.tsinghua.edu.cn

**Jingzhao Zhang**<sup>\*,†</sup>

jzhzhang@mit.edu

**Yanan Wang**<sup>\*,‡</sup>

wangyn7@mail.tsinghua.edu.cn

**Benben Jiang**<sup>\*,§</sup>

bbjiang@tsinghua.edu.cn

**Shaobo Huang**<sup>¶</sup>

huangshaobo@thinkenergy.net.cn

**Chen Wang**<sup>||</sup>

wangchen512@buaa.edu.cn

**Yang Zhang**<sup>§</sup>

zhangyang@thinkenergy.net.cn

**Xuebing Han**<sup>\*,\*\*</sup>

hanxuebing@tsinghua.edu.cn

**Dongxu Guo**<sup>‡</sup>

guodongxu@tsinghua.edu.cn

**Guannan He**<sup>†††</sup>

gnhe@pku.edu.cn

**Minggao Ouyang**<sup>†,\*\*</sup>

ouymg@tsinghua.edu.cn

## Abstract

We study the hypothesis testing problem for unknown dynamical systems. More specifically, we observe sequential input and output data from a dynamical system with unknown parameters, and we aim to determine whether the collected data is from a null distribution. Such a problem can have many applications. Here we formulate anomaly detection as hypothesis testing where the anomaly is defined through the alternative hypothesis. Consequently, hypothesis testing algorithms can detect faults in real-world systems such as robots, weather, energy systems, and stock markets. Although recent works achieved state-of-the-art performances in these tasks with deep learning models, we show that a careful analysis using hypothesis testing and graphical models can not only justify the effectiveness of autoencoder models, but also lead to a novel neural network design, termed DyAD (DYnamical system Anomaly Detection), with improved performances. We then show that DyAD achieves state-of-the-art performance on several existing datasets and a new dataset on battery anomaly detection in electric vehicles.

---

<sup>\*</sup>Equal contribution.

<sup>†</sup>IIS, Tsinghua University

<sup>‡</sup>State Key Laboratory of Automotive Safety and Energy, Tsinghua University

<sup>§</sup>Department of Automation, Tsinghua University

<sup>¶</sup>Beijing Circue Energy Technology Co., Ltd.

<sup>||</sup>School of Automation Science and Electrical Engineering, Beihang University

<sup>\*\*</sup>State Key Laboratory of Automotive Safety and Energy, Tsinghua University

<sup>††</sup>Department of Industrial Engineering and Management, Peking University

<sup>††</sup>Corresponding author.

## 1 Introduction

Hypothesis testing aims to decide whether the observed data supports or rejects a default belief known as the null hypothesis. Applications are abundant. In this work, we view anomaly detection as an application of hypothesis testing. This perspective is nothing profound—samples from the null hypothesis can be viewed as in-distribution, and rejection can be viewed as detecting anomalies. Despite being rather straightforward, this view was not carefully investigated in large-scale anomaly detection tasks that involve image data or long sequential data, because most classical hypothesis testing methods suffer from the curse of dimensionality.

To address the problem caused by high dimensionality, deep learning models naturally came in and lead to state-of-the-art anomaly detection power in both image data [26, 23, 38] and time series data [12, 29, 39, 6]. These methods are mostly motivated from diverse ideas but not from statistical testing.

In this work, we re-examine the statistical view of anomaly detection. We show that if we view anomaly detection as hypothesis testing and neural network training as a variational inference problem, then the very popular autoencoder method for anomaly detection can be viewed as likelihood ratio tests. Up to our knowledge, this establishes a first mathematical justification for the effectiveness of autoencoders in anomaly detection.

Furthermore, we show that this statistical view can readily adapt general autoencoder models to time-series data by exploiting a more refined graphical model for data collected from random dynamical systems. Specifically, we can develop a new autoencoder-based algorithm termed DyAD (DYnamical system Anomaly Detection). We show that the DyAD model achieves state-of-the-art performances on public datasets including MSL (Mars Science Laboratory rover) [12], SMAP (Soil Moisture Active Passive satellite) [20], and SWaT (Secure Water Treatment) [17].

To further validate our finding, we then release a much larger (roughly 50 times in terms of data points) dataset to benchmark several popular baselines. Our released dataset focuses on the battery safety problem in electric vehicles. In recent years, electric vehicle (EV) adoption rates increased exponentially due to their environmental friendliness, improved cruise range, and reduced costs brought by onboard lithium batteries [27, 18]. Yet, large-scale battery deployment can lead to unexpected fire incidents and product recalls [7]. Hence, accurately evaluating the health status of EV batteries is crucial to the safety of drivers and passengers. To promote research in this field, the dataset is collected from 301 electric vehicles recorded over three months to three years. Only battery-related data at charging stations was released for anonymity purposes. 50 of the 301 vehicles eventually suffered from battery failure. Experiments on the EV battery dataset confirm that our proposed model achieves better performance for system anomaly detection.

In summary, the outline of our work is as follows,

- We formulate hypothesis testing on data observed from dynamical systems under different graphical models. We then establish the connection between time series anomaly detection and hypothesis testing.
- We show that the above formulation, when applied with generalized likelihood ratio and variational inference, can justify the effectiveness of autoencoder models in anomaly detection.
- With a simple change to the underlying graphical model, we can design a novel neural network pipeline, termed DyAD, for anomaly detection on dynamical systems. We benchmark our proposed model on several existing time-series anomaly detection tasks and show that it achieves state-of-the-art performances.
- We further test our method on our new large-scale dataset collected from 301 electric vehicles. In addition to benchmarking anomaly detection algorithms, the dataset may be of independent interest for machine learning tasks in nonlinear systems.

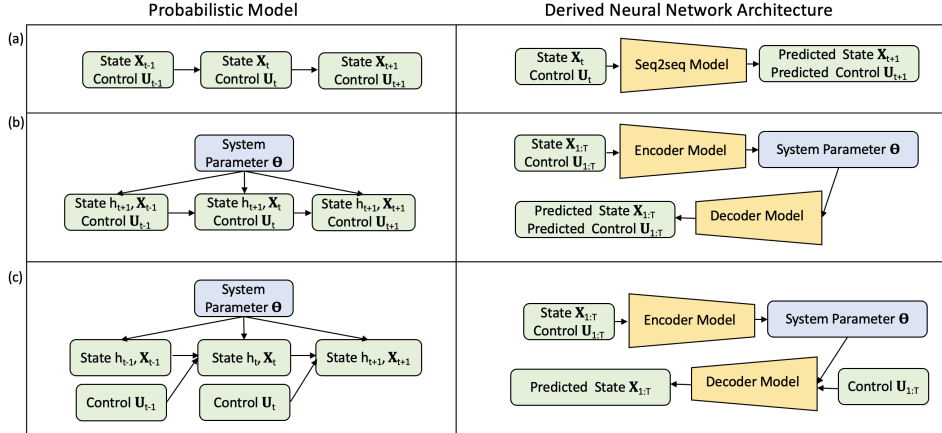


Figure 1: In the left column, we demonstrate the graphical models presented in Section 3.1. We illustrate the graphical models defined in (1), (2), and (3), respectively, in subplots (a), (b), (c). In the right column, we present the derived neural network models for anomaly detection following the analyses in Section 4. The model in row (b) can be viewed as a special case of row (c) where the control input is empty. The model in row (a) can be viewed as a special case of row (c) when the system parameter is dummy (e.g., encoder model is a constant function).

## 2 Related Works

### 2.1 Anomaly detection

Most works on anomaly detection (AD) starts from image datasets. Some previous works find that the model output probability for normal samples is higher [10, 9] in image tasks. Some previous works focus on detecting anomalies in the feature space by forcing/assuming the feature concentration of normal samples [28, 14]. Some enhance the representation power of networks by introducing contrastive learning [31, 30] and data transformation [9]. [21] partition the input into semantic and background parts and define the log-likelihood difference between a normal model and a background model as the likelihood ratio to distinguish anomalies. More recently, [22] propose a self-supervised neural network composed of masked convolutional layers and channel attention modules for vision tasks, which predicts a masked region in the convolutional receptive field. [24] utilize a memory bank learned from nominal samples and nearest neighborhood search to detect anomalies on industrial images. We refer readers to [3, 35] for a very thorough discussion of different algorithms.

Several recent works focus on time series anomaly detection. [16] propose to model reconstruction probabilities of the time series with an LSTM encoder-decoder network and use the reconstruction errors to detect anomalies. [12] leverage the prediction errors of the LSTM model to detect telemetry anomaly data. [29] propose OmniAnomaly to find the normal patterns through a stochastic recurrent neural network and use the reconstruction probabilities to determine anomalies. [39] capture multivariate correlations by considering each univariate series as an individual feature and including two graph attention layers to learn the dependencies of multivariate series in both temporal and feature dimensions. [6] adopt graph neural networks to learn the inter-variable interactions.

### 2.2 Electric vehicle fault detection

To the best of our knowledge, there is no deep learning study of battery system failure with large-scale datasets. On one hand, deep learning technology may not have been widely used in detecting battery failure, and many studies still use statistical methods [34] or canonical machine learning [40]. [32] add a bifunctional separator inside the battery to achieve early detection of lithium dendrites. [37] design a thermally modulated LFP (lithium iron phosphate) battery to improve cruise range.

On the other hand, deep learning based algorithms are applied but not verified on large-scale datasets. We notice that [15] collects data from 9 vehicles and divides them into three categories, [11] record time series information of one electric taxi, [40] use four cells with inconsistent capacities, and

[36] use eight cells. [11] adopt an LSTM network to predict multi-forward-step voltage value and judges the battery safety with a threshold voltage value. [15] propose to achieve higher battery fault diagnosis reliability and accuracy by combining the LSTM model and the equivalent circuit model. [36] employ multi-layer neural network to estimate the current of the short-circuited cell and then predict maximum temperature increase with a 3D electro-thermal coupling model.

### 3 Hypothesis Testing for Unknown Systems

In this section, we first introduce three different probabilistic graphical models for data collected from a dynamical system with different system parameters. We then show how time series anomaly detection can be formulated as hypothesis testing on unknown dynamical systems. Although most likely, none of the three models are exactly accurate for real-world applications, we will later show that different graphical models can lead to different anomaly detection algorithms, and that some models can perform better than the others on public datasets.

#### 3.1 Probabilistic models for random dynamical systems

One of the most basic graphical model (as in Figure 1a) for time series data could be the Markovian chain model below

$$\begin{aligned} h_{t+1} &= F(h_t), \\ X_{t+1} &\sim G(h_{t+1}) + \epsilon_t(x_t), \end{aligned} \quad (1)$$

where  $h_t \in \mathcal{H} \subseteq \mathbb{R}^d$  denotes the hidden system state,  $x_t \in \mathcal{X} \subseteq \mathbb{R}^d$  denotes the system output,  $G(h_t)$  describes the system output as a function of the hidden state,  $F(h_t)$  describes the deterministic part of the system dynamics, and  $\epsilon_t$  describes the randomness and noise. Note that we used the upper-case to denote the random variable, and the lower-case to denote the instantiated value.

The above model is natural if we consider the observed trajectory of a robot or the sensor states of a quadrotor. However, it cannot describe different system dynamics if the data comes from different systems, such as prices from different stocks or weather records collected in different seasons. This observation can lead to a second probabilistic model as illustrated in Figure 1b,

$$\begin{aligned} \theta \in \Theta, \quad h_{t+1} &= F(h_t, \theta), \\ X_{t+1} &\sim G(h_{t+1}) + \epsilon_t(h_{t+1}, \theta), \end{aligned} \quad (2)$$

where the system dynamic  $F(\cdot, \theta)$  and noise  $\epsilon_t(\cdot, \theta)$  are parameterized by  $\theta$ . In this way, different system parameters could encode information on the collected data. For example, if  $x_1, x_2, \dots, x_T$  denotes the time-series weather records, then  $\theta$  may contain information about the location, season and altitude.

The above probabilistic model, as we will later see, can already lead to effective deep learning models for anomaly detection. However, another limitation could be that it treats all the dimension of a piece of time-series data  $x_t \in \mathbb{R}^d$  equally, yet, we know that in dynamical system, control inputs are very often separated from internal states. If we further assume that the input is independent from the states, we get another probabilistic model with additional structure as in Figure 1c,

$$\begin{aligned} \theta \in \Theta, \quad U_{1:T} &\sim \mu_u, \quad h_{t+1} = F(h_t, u_t, \theta), \\ X_{t+1} &\sim G(h_{t+1}) + \epsilon_t(h_{t+1}, \theta), \end{aligned} \quad (3)$$

where  $x_t \in \mathcal{X} \subseteq \mathbb{R}^d$  denotes the system state,  $u_t \in \mathcal{U} \subseteq \mathbb{R}^{d'}$  denotes the control input.

We note that the above model is not necessarily a more accurate description of the data than the model in Figure 1b. However, in human-made dynamical systems, some dimensions, such as the charging current of a battery or moving direction of a robot, can be more dependent on human instructions than on the sensors. We will later see that in several applications, this model leads to better performance compared to the other two in anomaly detection.

#### 3.2 Hypothesis testing and anomaly detection in dynamical systems

In this subsection, we formulate time series anomaly detection as hypothesis testing in dynamical systems. For simplicity, we consider a discrete dynamical system with a fixed time length in a

Euclidean space. Recall the following notations that at each timestamp  $t$  we have an inner state  $x_t \in \mathcal{X}$ , a system input  $u_{1:t} \in \mathcal{U}$ , and a time-invariant system parameter  $\theta \in \Theta$ . Our goal is to detect whether an observed sample comes from a normal system, (i.e., from the null hypothesis  $H_0$ ), or from an abnormal system, (i.e., from the alternative hypothesis  $H_1$ ):

$$H_0 : (X_{1:T}, U_{1:T}, \theta) \sim \mu_0, \text{ for some } \mu_0 \in \mathcal{P}_0,$$

$$H_1 : (X_{1:T}, U_{1:T}, \theta) \sim \mu_1, \text{ for some } \mu_1 \in \mathcal{P}_1.$$

The above formulation subsumes many real-world problems. For example, if we aim to detect abnormal electric vehicle batteries,  $\theta$  can describe battery mechanism, whereas the signals  $x_t$  are recorded by the battery management system under the charging current  $u_t$ . The distribution  $\mu_0$  describes the distribution of healthy batteries, whereas  $\mathcal{P}$  contains the potential abnormal/unhealthy batteries.

The above problem *cannot* be solved directly for many reasons. First, the system parameter  $\theta$  is unknown and needs to be figured out from the data. Second, we do not have the exact characterization of the distributions of  $U$  and  $X$ . Instead, as in many machine learning problems, we have i.i.d samples as a surrogate. In the next section, we show how with reasonable assumptions, solving the hypothesis testing problem can lead to training an autoencoder model.

## 4 Autoencoders: Testing via Likelihood Ratio and Learning via Variational Inference

Autoencoders (see the right column of Figure 1b) are widely used for anomaly detection tasks [1, 16, 3]. The intuition was that due to limited dimension of the latent space, an encoder-decoder model should only record the most common patterns in the data. Hence, infrequent patterns will generate large reconstruction errors and be identified as anomalies. In this section, we show that the above intuition can be made rigorous from the hypothesis testing perspective.

Our analysis focuses on the third graphical model (3) as shown in Figure 1c. The second model (2) in Figure 1b can be viewed as a special case of Figure 1c when the control input is empty; therefore, our derivation subsumes the design of regular Autoencoder models.

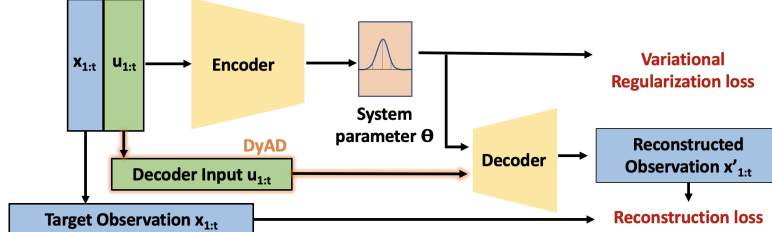


Figure 2: The training pipeline for the proposed DyAD model. The orange shade highlights the difference between DyAD and a standard VAE model.

### 4.1 Model prediction: Generalized likelihood ratio test

Before we move on to describe the neural network architecture, we hope to motivate why obtaining an anomaly detection model requires solving a variational inference problem. This would become clear if we use the generalized likelihood ratio test. When the likelihood can be calculated, the log generalized likelihood ratio of the form,

$$\lambda(x_{1:T}, u_{1:T}) := \log \left( \frac{\sup_{\theta \in \Theta} p_0(x_{1:T}, u_{1:T} | \theta)}{\sup_{\theta \in \Theta} p_1(x_{1:T}, u_{1:T} | \theta)} \right), \quad (4)$$

is among the most popular hypothesis testing technique. Its false discovery rate can be bounded by Wilk's theorem under regularity conditions. The exact asymptotic distribution of a generalized likelihood ratio depends on conditions of the actual underlying distribution. We leave a more exact characterization as future work but instead focus on providing a tractable way to compute the ratio.

To do so, we need to specify the null and alternative hypothesis classes  $\mathcal{P}_0$  and  $\mathcal{P}_1$ . In view of the graphical model in (3), we only need to specify three terms,

1.  $f_\theta(\cdot) = G(F(\cdot, \theta))$  is a recurrent deep sequence-to-sequence model (e.g., LSTM, RNN, GRU) that maps a control input  $u_t$  and a hidden state  $h_t$  to the next predicated output  $x_{t+1}$  and state  $h_{t+1}$ .
2. The system parameter  $\theta$  is a vector (instead of the network weights) fed into the deep model to determine the output. One example is as shown in the right column of Figure 1.
3. The noise  $\epsilon_t(h_t, \theta) \sim \mathcal{N}(0, \sigma^2 I)$  for all  $h_t, \theta$ . The only difference between the null and alternative hypothesis classes  $\mathcal{P}_0$  and  $\mathcal{P}_1$  is that the noise in null hypothesis  $\sigma_0^2$  is smaller than that in the alternative hypothesis  $\sigma_1^2$ .

*Remark 4.1.* We make two remarks on the validity of the above assumptions.

1. *The first two assumptions are quite general given the expressivity of neural networks. The third assumption on noise, however, seems very restrictive. We believe that a more general model where the noise is state-dependent can lead to better predictions with larger datasets, and we leave this as a future work when more larger scale data can be available.*
2. *The key difference between the null hypothesis and alternative hypothesis is that that a normal system sampled from the null hypothesis could have smaller observed noise, as the system can predict future events better. We will later see that the exact value of  $\sigma_0$  and  $\sigma_1$  does not matter as it only changes the threshold of likelihood ratio. In fact, via a monotone likelihood ratio argument, we can relax the hypothesis classes to  $\sigma_0 \leq \sigma^*$  and  $\sigma_1 > \sigma^*$  for any fixed  $\sigma^*$ .*

After defining the hypothesis classes, we can finally simplify the likelihood assuming that we observe the data  $x_{1:T}, u_{1:T}$ . Let  $p_0(x_{1:T}, u_{1:T} | \theta)$  denote the probability distribution under null hypothesis  $\mu_0 \in \mathcal{P}_0$ , and  $p_1(x_{1:T}, u_{1:T} | \theta)$  that of the alternative hypothesis for some  $\mu_1 \in \mathcal{P}_1$ . We get by Bayesian rule and the graphical model in Figure 1c that

$$p_i(x_{1:T}, u_{1:T} | \theta) = p(u_{1:T}) \prod_{t \leq T} p_i(x_{t+1} | u_t, h_t, \theta)$$

for  $i \in \{0, 1\}$ . Note that the distribution of the control is not dependent on  $i$ . Then by the Gaussian noise assumption, the log-likelihood can be written as

$$l_0(x_{1:T}, u_{1:T} | \theta) = \log(p(u_{1:T})) - \frac{1}{\sigma_0^2} \sum_{t \leq T} (f_\theta(u_t, h_t) - x_{t+1})^2. \quad (5)$$

We note that both the null and alternative likelihoods achieve maximal at the same parameter

$$\begin{aligned} \hat{\theta} &:= \arg \max_{\theta \in \Theta} l_1(x_{1:T}, u_{1:T} | \theta) \\ &= \arg \max_{\theta \in \Theta} l_0(x_{1:T}, u_{1:T} | \theta). \end{aligned}$$

Then by (4), the generalized likelihood ratio can be written as

$$\lambda(x_{1:T}, u_{1:T}) := \frac{\sigma_1^2 - \sigma_0^2}{\sigma_0^2 \sigma_1^2} \sum_{t \leq T} (f_{\hat{\theta}}(u_t, h_t) - x_{t+1})^2. \quad (6)$$

This means that we can detect the anomaly of an observed sequence  $x_{1:T}, u_{1:T}$  with a classifier  $c : x_{1:T}, u_{1:T} \rightarrow \{0, 1\}$  by computing the generalized likelihood ratio test, which in view of (6) is simply thresholding the squared error

$$c(x_{1:T}, u_{1:T}) = \mathbb{I}\left\{\sum_{t \leq T} (f_{\hat{\theta}}(u_t, h_t) - x_{t+1})^2 \geq \tau\right\}.$$

Therefore, to achieve the efficiency of the generalized likelihood ratio test, we only need to figure out the mapping  $f_\theta$  and the MLE estimator  $\hat{\theta}$ . We specify the procedure in the next subsection.

Table 1: F1, Precision and Recall on the two spacecraft datasets. Bold denotes the best results.

Method	MSL			SMAP			SWaT		
	F1	Precision	Recall	F1	Precision	Recall	F1	Precision	Recall
AE	0.5774	0.5507	0.6070	0.6215	0.8606	0.4864	0.7961	0.9452	0.6876
Deep SVDD	0.6804	0.8270	0.5779	0.2965	0.1752	0.9630	0.7870	0.8633	0.7231
LSTMAD	0.4502	0.3831	0.5458	0.6944	0.8914	0.5687	0.8007	0.9570	0.6883
MTAD-GAT	0.9084	0.8754	0.9440	0.9013	0.8906	0.9123	0.8359	0.9271	0.7612
GDN	0.7660	0.7598	0.7723	0.7069	0.7556	0.6641	0.8082	0.9935	0.6812
<b>DyAD (Ours)</b>	<b>0.9438</b>	0.9215	0.9673	<b>0.9313</b>	0.9501	0.9132	<b>0.8399</b>	0.9824	0.7335

## 4.2 Model training: Variational inference

Recall from the previous subsection that we want to specify two mappings to compute the generalized likelihood ratio test. We denote the first one

$$g_e : u_{1:T} \times x_{1:T} \rightarrow \theta$$

as the encoder function that finds the MLE estimator  $\hat{\theta}$  given a sequence of observations. We denote the second one

$$g_d : \theta \times u_t \times h_t \rightarrow x_{t+1} \times h_{t+1}$$

as the decoder function that maps the system parameter  $\theta$  and control input to a sequence of expected system output. Note that the decoder naturally has a recurrent structure and can be parameterized by neural networks including GRU, LSTM or RNN. Ideally,  $g_d$  should coincide with the ground truth dynamics

$$g_d(u_t, h_t, \theta) = f_\theta(u_t, h_t).$$

The desired property of  $g_e$  is that they solve the MLE problem in (5). Together, this gives the training objective below

$$\min_{g_e, g_d} \sum_{t \leq T} (g_d(u_t, h_t, g_e(u_{1:T}, x_{1:T})) - x_{t+1})^2$$

Solving the above directly would give the standard autoencoder objective. However, this problem is not well defined as the solution is underdetermined. The value of  $\theta$  can be reparametrized (e.g., scaling up  $g_e$  by 2) arbitrarily due to the redundancy in  $g_d$  (e.g., scaling down  $g_d$  by 2) without changing the system dynamics.

Therefore, we add an additional constraint that  $\theta \sim \mathcal{N}(0, I)$ . Then given an observed sequence  $u_{1:T}, x_{1:T}$ , instead of directly maximizing the log likelihood, the surrogate objective would look like below using the evidence lower bound (ELBO) trick (see [13, 8]),

$$\begin{aligned} \text{ELBO} = & \mathbb{E}_{\theta \sim p_0(\theta|x_{1:T}, u_{1:T})} [l_0(x_{1:T}, u_{1:T}|\theta)] \\ & + D_{KL}(p_0(\theta|x_{1:T}, u_{1:T}) \parallel \mathcal{N}(0, I)), \end{aligned} \quad (7)$$

where  $D_{KL}$  is the KL divergence.

The posterior distribution  $p_0(\theta|x_{1:T}, u_{1:T})$  in general is not computable. Hence, we adopt the variational inference perspective and parameterize the potential posterior distribution as below,

$$p_0(\theta|x_{1:T}, u_{1:T}) = \mathcal{N}(\mu, \sigma),$$

where  $\mu, \sigma = g_e(u_{1:T}, x_{1:T})$ . Hence we can simplify the second term in ELBO using the KL-divergence between Gaussians

$$\begin{aligned} D_{KL}(p_0(\theta|x_{1:T}, u_{1:T}) \parallel \mathcal{N}(0, I)) \\ = \|\mu\|^2 + \text{tr}(\sigma^2) - \log(|\sigma^2|). \end{aligned}$$

We also further simplify the first term in ELBO with (5). Then to maximize ELBO (7), it is equivalent to solve the problem below

$$\begin{aligned} \max_{g_e, g_d} & \underbrace{\|\mu\|^2 + \text{tr}(\sigma^2) - \log(|\sigma^2|)}_{\text{variational regularization loss}} + \underbrace{\mathbb{E}_{\theta \sim \mathcal{N}(\mu, \sigma)} \left[ \sum_{t \leq T} (g_d(u_t, h_t, \theta) - x_{t+1})^2 \right]}_{\text{reconstruction loss}} \\ \text{s.t. } & \mu, \sigma = g_e(u_{1:T}, x_{1:T}) \end{aligned} \quad (8)$$

This leads to an objective that is very similar to the one in variational autoencoder (VAE), **except for the additional  $u_t$  term in the decoder**. It contains a reconstruction loss and a variational regularization loss, as summarized in Figure 2. Hence, we can train the neural network following the same procedure as VAE by solving an empirical risk minimization problem using  $n$  i.i.d samples.

*Remark 4.2.* Our analysis above is not much different from the original work on variational autoencoder [13]. We include a concise derivation for completeness, and we refer readers to the original work [13] for a more detailed discussion.

The key difference of the proposed DyAD model against a standard autoencoder model is highlighted in Figure 2 with orange shadow. This difference is not substantial in implementation. However, in later experiments, we show that on several public datasets, this graphical-model motivated modification can significantly improve model performance.

	MSL	SMAP	SWaT	EV (ours)
# dimensions	55	25	50	8
# time frames	132, 046	562, 800	92, 255	88, 135, 040
Anomaly ratio	10.27%	13.13%	5.95%	N/A

Table 2: The statistics of the four datasets used in the experiments.

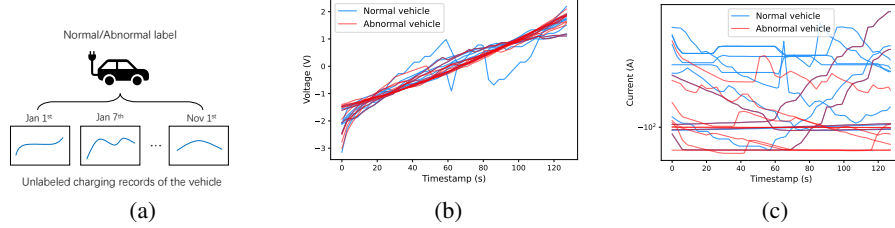


Figure 3: An illustration of our EV dataset. (a) The data structure of our EV dataset. Only vehicle-level anomaly labels are available. Charging snippets are collected within months and years. (b)-(c) The voltage and current of charging snippets collected from a normal and an abnormal vehicle.

## 5 Benchmark DyAD on Public Datasets

In this section, we benchmark the proposed DyAD model against several popular algorithms in time-series anomaly detection tasks. Our results suggest that, although autoencoder models have been outperformed by more recent algorithms, our proposed variation, the DyAD model, can again lead to state-of-the-art results.

The three public datasets we used are MSL (Mars Science Laboratory rover), SMAP (Soil Moisture Active Passive satellite) and SWaT (Secure Water Treatment). The first two are spacecraft system time-series anomaly detection datasets released by NASA [20, 12]. They record the spacecrafts' telemetry channel sequences and command sequences encoded as 0 or 1. The last one is a water treatment dataset integrates digital and physical elements to control and monitor system behaviors. They are widely used as benchmarks for anomaly detection [12, 39, 4, 6]. The size of all datasets are summarized in Table 2. We note that all three datasets have at least a dimension in the time series that records the input from human-intervention. In spacecrafts, it is named ‘‘command sequence’’, and in the water treatment system, it is named ‘‘actuator dimension’’. We believe that this structure results in the efficiency of our proposed DyAD model.

We compare our model against five different algorithms, including autoencoder (AE) [1], Deep SVDD [25], LSTMAD [16], MTAD-GAT [39], and GDN [6]. We measure anomaly detection with commonly used metrics: F1 score, Precision, and Recall. The experiment results are shown in Table 1. For the spacecraft system, we treat the command dimensions as system inputs and the telemetry data as system responses. As shown in the table, DyAD achieves the best F1 scores consistently. Specifically, we improve the SOTA algorithm by 3.9% and 3.0% on the MSL and SMAP datasets respectively. For the water treatment system, the sensor dimensions are treated as system inputs and

the actuator dimensions as system responses. We can see from the table that DyAD outperforms other baseline algorithms by 0.4%. More implementation details can be found in Appendix B.

## 6 Battery system anomaly detection

We further test all the algorithms on a new dataset that we collect from real world electric vehicle (EV) records. Before we present the anomaly detection results, we briefly describe our released EV dataset. Due to the wide range of applications and great significance of the EV battery, we release a large-scale battery dataset, which contains over 88M battery charging time steps collected from 301 vehicles (see detailed stats in Table 2). The multi-dimensional time series features include current, voltage, temperature and SOC (state of charge) information. An example is shown in Figure 3(b) and 3(c). More examples can be found in Appendix A. Our dataset and code are available upon request. The usage of our data is under CC BY-NC-SA license.

We highlight that unlike previous datasets where anomalies are marked when an unexpected event happens in time series, the anomaly labels in the EV dataset have a natural hierarchical structure as shown in Figure 3(a). Specifically, as shown in Figure 3(b) the abnormality labels are at the vehicle level (one per vehicle) rather than the event level (one per timestamp), which is a more challenging time series anomaly detection task. To address the problem, we adopt the following procedure to summarize piece-wise prediction into vehicle-level prediction.

**Detect vehicle level anomalies** To handle the hierarchical dataset structure and sparsity of anomaly labels, we propose a robust scoring function to map the snippet-level scores obtained from DyAD to vehicle-level predictions, shown in Alg. 1. In particular, we predict the abnormal degree of a charging snippet by thresholding the reconstruction error at value  $\tau$  and then predict whether a vehicle is abnormal by averaging the top  $h$  percentile errors. Both  $\tau$  and  $h$  are fine-tuned on the validation dataset. We apply both the robust scoring function to all deep learning baselines.

---

**Algorithm 1** Pseudo code of the robust scoring function

---

**Hyperparameters:** percentile  $h$  and threshold  $\tau$ .  
**Input:** Charging snippet scores  $\vec{r} = \{(r_i)\}_i$  from a vehicle.  
**Output:** Vehicle level prediction.

- 1: Sort  $\vec{r}$  by  $r_i$  from large to small.
- 2: Take the mean of the largest  $h\%$  as the vehicle’s score.
- 3: Predict a vehicle as abnormal if the average of the largest  $h\%$  is greater than  $\tau$ .

---

### 6.1 Experiment results

On this dataset, we see that the proposed algorithm, DyAD, outperforms other algorithms significantly. To highlight the difference, we compare different algorithms in terms of the receiver operating characteristic(ROC) curve. Both accuracy and recall can be read off from the curve via selecting different thresholds.

We plot the averaged ROC curves out of 5-fold cross-validation. The mean and variance of AUROC values are shown in Figure 4 and Table 3, respectively. Our proposed algorithm DyAD achieves the best performance on our large-scale dataset against well-established autoencoder-based and graph-based algorithms. Meanwhile, this is the first time to deploy deep learning algorithms to detect electric vehicle battery system failure in such a large dataset.

We further examine the difficulty of detecting anomalies in each make by *training models on data from the same make only*. Make 3 is omitted since it has only four anomaly vehicles thus can not do the five-fold cross-validation. The AUROC values of different algorithms are shown in Table 4. It seems that learning one make of vehicles individually would lead to a larger variance of the results. One possible reason is due to the smaller amount of data. When the variance of the results becomes significantly larger, the mean value of the results becomes less reliable in comparing different algorithms affected by outlier values. Therefore, we recommend using a larger number of vehicles to reflect the performance of the algorithms in the population. In all five algorithms, the variance of DyAD, although also increased, is still at a lower level than the other four. Based on the

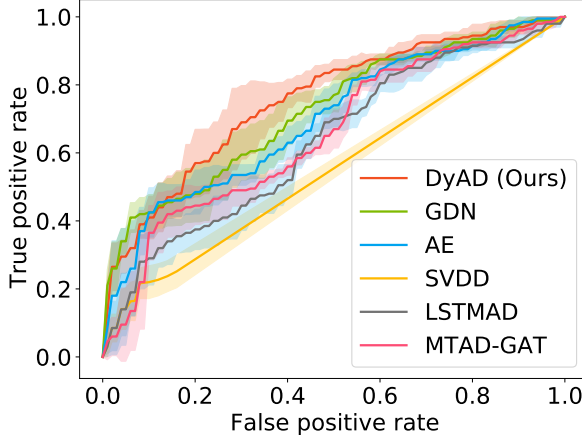


Figure 4: Interpolated averaged ROC curves of several algorithms on our EV battery dataset. Shaded area represents the five-fold variance.

Table 3: Mean and standard variance of *test* AUROC (%) values on all vehicles from three makes. Among all the considered algorithms, DyAD achieves the best detection results by a 3.1%  $\sim$  20.0% AUROC boost and a relatively small variance compared to the second best algorithm. Bold denotes the best results.

Algorithm	AUROC (%) by Robust Score
AE	$69.4 \pm 2.6$
Deep SVDD	$55.2 \pm 2.5$
LSTMAD	$63.1 \pm 1.7$
MTAD-GAT	$65.2 \pm 2.3$
GDN	$72.1 \pm 3.2$
<b>DyAD (Ours)</b>	<b><math>75.2 \pm 2.7</math></b>

results in Table 4, detecting anomalous vehicles from Make 2 appears to be simpler than that from Make 1.

By comparing Table 4 against Table 3, we notice that some algorithms (e.g., GDN) benefit from training on all vehicles altogether, whereas some (e.g., DyAD) benefit from learning different models for each Make. Hence, there is still room for researchers to improve the detection of electric vehicle battery system failure. Limited to time and computing resources, we only implement these algorithms. We also welcome researchers to further develop algorithms on the dataset to improve EV safety.

## 7 Conclusions and discussions

In this work, we first establish the natural connection between anomaly detection and hypothesis testing. We then show that this view can justify the effectiveness of autoencoder models as they are equivalent to generalized likelihood ratio tests with different assumptions on the underlying graphical models of the data distribution.

Next, we show that properly formulating the probabilistic model underlying the data—in our case, viewing time series as outputs from dynamical systems—can greatly improve sample efficiency and lead to better model design. Our analysis naturally motivates a variant of the autoencoder model that is tailored for dynamical systems. The performance of our proposed model is validated on both our released large-scale EV dataset and on existing public datasets.

There is much to be done. First, our model has very restrictive assumptions on the noise distribution. Proposing a new model under more generalized noise distribution might lead to novel and powerful anomaly detection models. Second, it is known that models based on likelihood alone do not achieve the best performances, as observed in [19]. The idea is that although likelihood provides a guarantee

Table 4: Mean and standard variance of *test* AUROC (%) values on each make. Bold denotes the best results.

Algorithm	Make 1	Make 2
AE	$65.3 \pm 7.0$	$59.4 \pm 8.4$
Deep SVDD	$51.6 \pm 5.7$	$58.5 \pm 13.7$
LSTMAD	$56.0 \pm 7.3$	$58.6 \pm 9.5$
MTAD-GAT	$57.1 \pm 9.9$	$50.9 \pm 12.5$
GDN	$64.8 \pm 11.5$	$65.3 \pm 4.3$
<b>DyAD (Ours)</b>	<b><math>78.0 \pm 5.2</math></b>	<b><math>84.4 \pm 3.8</math></b>

of the false discovery rate, it does not necessarily give the best detection power, which would depend on the distribution of the alternative hypothesis. For this reason, multiple improvements [21, 33, 5] have been made to further boost detection performances by improving the scores generated by likelihoods. It remains to see whether similar ideas can be applied to improve our models.

## References

- [1] Charu C. Aggarwal. *Outlier Analysis*. Springer, 2013.
- [2] Chuadhy Mujeeb Ahmed, Venkata Reddy Palleti, and Aditya P. Mathur. WADI: a water distribution testbed for research in the design of secure cyber physical systems. In Panagiotis Tsakalides and Baltasar Beferull-Lozano, editors, *Proceedings of the 3rd International Workshop on Cyber-Physical Systems for Smart Water Networks, CySWATER@CPSWeek 2017, Pittsburgh, Pennsylvania, USA, April 21, 2017*, pages 25–28. ACM, 2017.
- [3] Paul Bergmann, Michael Fauser, David Sattlegger, and Carsten Steger. Mvtec ad—a comprehensive real-world dataset for unsupervised anomaly detection. In *Proceedings of the IEEE/CVF conference on computer vision and pattern recognition*, pages 9592–9600, 2019.
- [4] Wenchao Chen, Long Tian, Bo Chen, Liang Dai, Zhibin Duan, and Mingyuan Zhou. Deep variational graph convolutional recurrent network for multivariate time series anomaly detection. In Kamalika Chaudhuri, Stefanie Jegelka, Le Song, Csaba Szepesvári, Gang Niu, and Sivan Sabato, editors, *International Conference on Machine Learning, ICML 2022, 17-23 July 2022, Baltimore, Maryland, USA*, volume 162 of *Proceedings of Machine Learning Research*, pages 3621–3633. PMLR, 2022.
- [5] Hyunsun Choi, Eric Jang, and Alexander A Alemi. Waic, but why? generative ensembles for robust anomaly detection. *arXiv preprint arXiv:1810.01392*, 2018.
- [6] Ailin Deng and Bryan Hooi. Graph neural network-based anomaly detection in multivariate time series. In *Thirty-Fifth AAAI Conference on Artificial Intelligence, AAAI 2021, Thirty-Third Conference on Innovative Applications of Artificial Intelligence, IAAI 2021, The Eleventh Symposium on Educational Advances in Artificial Intelligence, EAAI 2021, Virtual Event, February 2-9, 2021*, pages 4027–4035. AAAI Press, 2021.
- [7] Jie Deng, Chulheung Bae, James Marcicki, Alvaro Masias, and Theodore Miller. Safety modelling and testing of lithium-ion batteries in electrified vehicles. *Nature Energy*, 3(4):261–266, 2018.
- [8] Ming Ding. The road from mle to em to vae: A brief tutorial. *AI Open*, 2021.
- [9] Izhak Golan and Ran El-Yaniv. Deep anomaly detection using geometric transformations. In *NeurIPS 2018*, 2018.
- [10] Dan Hendrycks and Kevin Gimpel. A baseline for detecting misclassified and out-of-distribution examples in neural networks. *arXiv preprint arXiv:1610.02136*, 2016.
- [11] Jichao Hong, Zhenpo Wang, and Yongtao Yao. Fault prognosis of battery system based on accurate voltage abnormality prognosis using long short-term memory neural networks. *Applied Energy*, 251:113381, 2019.
- [12] Kyle Hundman, Valentino Constantinou, Christopher Laporte, Ian Colwell, and Tom Söderström. Detecting spacecraft anomalies using lstms and nonparametric dynamic thresholding. In Yike

Guo and Faisal Farooq, editors, *Proceedings of the 24th ACM SIGKDD International Conference on Knowledge Discovery & Data Mining, KDD 2018, London, UK, August 19-23, 2018*, pages 387–395. ACM, 2018.

- [13] Diederik P Kingma and Max Welling. Auto-encoding variational bayes. *arXiv preprint arXiv:1312.6114*, 2013.
- [14] Kimin Lee, Kibok Lee, Honglak Lee, and Jinwoo Shin. A simple unified framework for detecting out-of-distribution samples and adversarial attacks. In *NeurIPS 2018*, 2018.
- [15] Da Li, Zhaosheng Zhang, Peng Liu, Zhenpo Wang, and Lei Zhang. Battery fault diagnosis for electric vehicles based on voltage abnormality by combining the long short-term memory neural network and the equivalent circuit model. *IEEE Transactions on Power Electronics*, 36(2):1303–1315, 2020.
- [16] Pankaj Malhotra, Anusha Ramakrishnan, Gaurangi Anand, Lovekesh Vig, Puneet Agarwal, and Gautam Shroff. Lstm-based encoder-decoder for multi-sensor anomaly detection. *CoRR*, abs/1607.00148, 2016.
- [17] Aditya P. Mathur and Nils Ole Tippenhauer. Swat: a water treatment testbed for research and training on ICS security. In *2016 International Workshop on Cyber-physical Systems for Smart Water Networks, CySWater@CPSWeek 2016, Vienna, Austria, April 11, 2016*, pages 31–36. IEEE Computer Society, 2016.
- [18] Lukas Mauler, Fabian Duffner, Wolfgang G Zeier, and Jens Leker. Battery cost forecasting: a review of methods and results with an outlook to 2050. *Energy & Environmental Science*, 2021.
- [19] Eric Nalisnick, Akihiro Matsukawa, Yee Whye Teh, Dilan Gorur, and Balaji Lakshminarayanan. Do deep generative models know what they don’t know? *arXiv preprint arXiv:1810.09136*, 2018.
- [20] Peggy O’Neill, Dara Entekhabi, Eni G. Njoku, and Kent H. Kellogg. The NASA soil moisture active passive (SMAP) mission: Overview. In *IEEE International Geoscience & Remote Sensing Symposium, IGARSS 2010, July 25-30, 2010, Honolulu, Hawaii, USA, Proceedings*, pages 3236–3239. IEEE, 2010.
- [21] Jie Ren, Peter J Liu, Emily Fertig, Jasper Snoek, Ryan Poplin, Mark Depristo, Joshua Dillon, and Balaji Lakshminarayanan. Likelihood ratios for out-of-distribution detection. *Advances in neural information processing systems*, 32, 2019.
- [22] Nicolae-Cătălin Ristea, Neelu Madan, Radu Tudor Ionescu, Kamal Nasrollahi, Fahad Shahbaz Khan, Thomas B. Moeslund, and Mubarak Shah. Self-supervised predictive convolutional attentive block for anomaly detection. In *Proceedings of the IEEE/CVF Conference on Computer Vision and Pattern Recognition (CVPR)*, pages 13576–13586, June 2022.
- [23] Karsten Roth, Latha Pemula, Joaquin Zepeda, Bernhard Schölkopf, Thomas Brox, and Peter Gehler. Towards total recall in industrial anomaly detection. In *Proceedings of the IEEE/CVF Conference on Computer Vision and Pattern Recognition*, pages 14318–14328, 2022.
- [24] Karsten Roth, Latha Pemula, Joaquin Zepeda, Bernhard Schölkopf, Thomas Brox, and Peter Gehler. Towards total recall in industrial anomaly detection. In *Proceedings of the IEEE/CVF Conference on Computer Vision and Pattern Recognition (CVPR)*, pages 14318–14328, June 2022.
- [25] Lukas Ruff, Nico Görnitz, Lucas Deecke, Shoaib Ahmed Siddiqui, Robert A. Vandermeulen, Alexander Binder, Emmanuel Müller, and Marius Kloft. Deep one-class classification. In Jennifer G. Dy and Andreas Krause, editors, *Proceedings of the 35th International Conference on Machine Learning, ICML 2018, Stockholmsmässan, Stockholm, Sweden, July 10-15, 2018*, volume 80 of *Proceedings of Machine Learning Research*, pages 4390–4399. PMLR, 2018.
- [26] Lukas Ruff, Robert Vandermeulen, Nico Goernitz, Lucas Deecke, Shoaib Ahmed Siddiqui, Alexander Binder, Emmanuel Müller, and Marius Kloft. Deep one-class classification. In *International conference on machine learning*, pages 4393–4402. PMLR, 2018.
- [27] Richard Schmuck, Ralf Wagner, Gerhard Höpel, Tobias Placke, and Martin Winter. Performance and cost of materials for lithium-based rechargeable automotive batteries. *Nature Energy*, 3(4):267–278, 2018.
- [28] Bernhard Schölkopf, Robert C. Williamson, Alexander J. Smola, John Shawe-Taylor, and John C. Platt. Support vector method for novelty detection. In *NeurIPS 1999*, 1999.

[29] Ya Su, Youjian Zhao, Chenhao Niu, Rong Liu, Wei Sun, and Dan Pei. Robust anomaly detection for multivariate time series through stochastic recurrent neural network. In Ankur Teredesai, Vipin Kumar, Ying Li, Rómér Rosales, Evmaria Terzi, and George Karypis, editors, *Proceedings of the 25th ACM SIGKDD International Conference on Knowledge Discovery & Data Mining, KDD 2019, Anchorage, AK, USA, August 4-8, 2019*, pages 2828–2837. ACM, 2019.

[30] Jihoon Tack, Sangwoo Mo, Jongheon Jeong, and Jinwoo Shin. CSI: novelty detection via contrastive learning on distributionally shifted instances. In Hugo Larochelle, Marc’Aurelio Ranzato, Raia Hadsell, Maria-Florina Balcan, and Hsuan-Tien Lin, editors, *Advances in Neural Information Processing Systems 33: Annual Conference on Neural Information Processing Systems 2020, NeurIPS 2020, December 6-12, 2020, virtual*, 2020.

[31] Jim Winkens, Rudy Bunel, Abhijit Guha Roy, Robert Stanforth, Vivek Natarajan, Joseph R Led-sam, Patricia MacWilliams, Pushmeet Kohli, Alan Karthikesalingam, Simon Kohl, et al. Contrastive training for improved out-of-distribution detection. *arXiv preprint arXiv:2007.05566*, 2020.

[32] Hui Wu, Denys Zhuo, Desheng Kong, and Yi Cui. Improving battery safety by early detection of internal shorting with a bifunctional separator. *Nature communications*, 5(1):1–6, 2014.

[33] Zhisheng Xiao, Qing Yan, and Yali Amit. Likelihood regret: An out-of-distribution detection score for variational auto-encoder. *Advances in neural information processing systems*, 33:20685–20696, 2020.

[34] Qiao Xue, Guang Li, Yuanjian Zhang, Shiquan Shen, Zheng Chen, and Yonggang Liu. Fault diagnosis and abnormality detection of lithium-ion battery packs based on statistical distribution. *Journal of Power Sources*, 482:228964, 2021.

[35] Jingkang Yang, Pengyun Wang, Dejian Zou, Zitang Zhou, Kunyuan Ding, Wenxuan Peng, Haoqi Wang, Guangyao Chen, Bo Li, Yiyou Sun, et al. Openood: Benchmarking generalized out-of-distribution detection. *arXiv preprint arXiv:2210.07242*, 2022.

[36] Ruixin Yang, Rui Xiong, Suxiao Ma, and Xinfan Lin. Characterization of external short circuit faults in electric vehicle li-ion battery packs and prediction using artificial neural networks. *Applied Energy*, 260:114253, 2020.

[37] Xiao-Guang Yang, Teng Liu, and Chao-Yang Wang. Thermally modulated lithium iron phosphate batteries for mass-market electric vehicles. *Nature Energy*, 6(2):176–185, 2021.

[38] Vitjan Zavrtanik, Matej Kristan, and Danijel Skočaj. Draem-a discriminatively trained reconstruction embedding for surface anomaly detection. In *Proceedings of the IEEE/CVF International Conference on Computer Vision*, pages 8330–8339, 2021.

[39] Hang Zhao, Yujing Wang, Juanyong Duan, Congrui Huang, Defu Cao, Yunhai Tong, Bixiong Xu, Jing Bai, Jie Tong, and Qi Zhang. Multivariate time-series anomaly detection via graph attention network. In Claudia Plant, Haixun Wang, Alfredo Cuzzocrea, Carlo Zaniolo, and Xindong Wu, editors, *20th IEEE International Conference on Data Mining, ICDM 2020, Sorrento, Italy, November 17-20, 2020*, pages 841–850. IEEE, 2020.

[40] Yuejiu Zheng, Yifan Lu, Wenkai Gao, Xuebing Han, Xuning Feng, and Minggao Ouyang. Micro-short-circuit cell fault identification method for lithium-ion battery packs based on mutual information. *IEEE Transactions on Industrial Electronics*, 68(5):4373–4381, 2020.

## A Dataset examples

Some charging snippets from the battery dataset are depicted in Figure 5. The feature dimensions include voltage, current, max/min single cell voltage and max/min cell temperature. From the figure, we can see that the time series are mixed, and there is no simple rule to distinguish the charging snippets of abnormal vehicles from normal charging snippets. This is also one of the main reasons why anomaly labels are on the vehicle level rather than the snippet level.

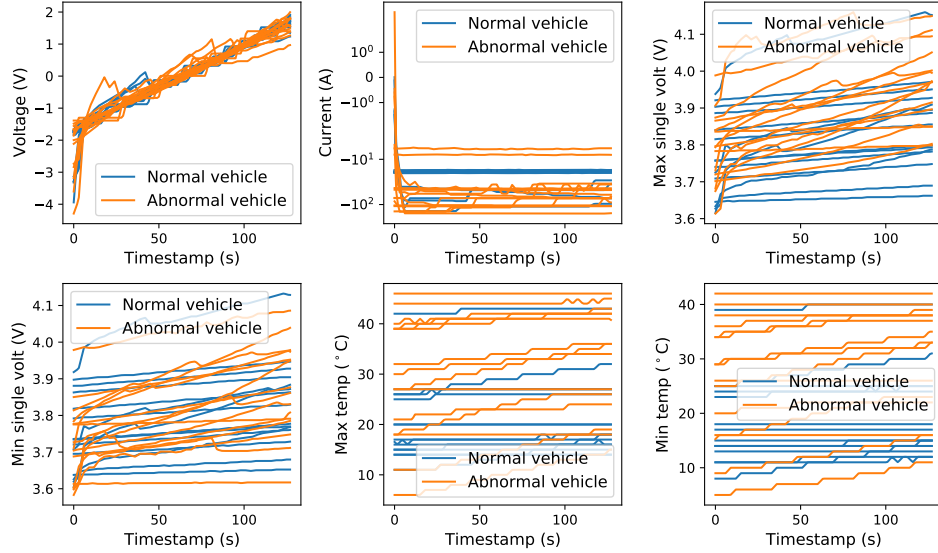


Figure 5: Charging snippet examples from snippets of normal and abnormal vehicles.

Here we also give a conceptual figure to help to understand what an anomaly in battery system would be like. In Figure 6, there are three charging snippets collected from a vehicle, where the first two have a normal max temperature value and the third shows a sharp increase in temperature. Notice that the different snippets are not contiguous, and there are discharging phase between snippets. Our dataset does not contain the third type of snippets, as our goal is to detect battery system failures early enough to prevent potential hazard in advance.

This example also explains that the labels in the dataset can only be labeled at the vehicle level, but not at the charging snippet level, since even a battery system that is about to fail may exhibit a normal charging pattern early on.

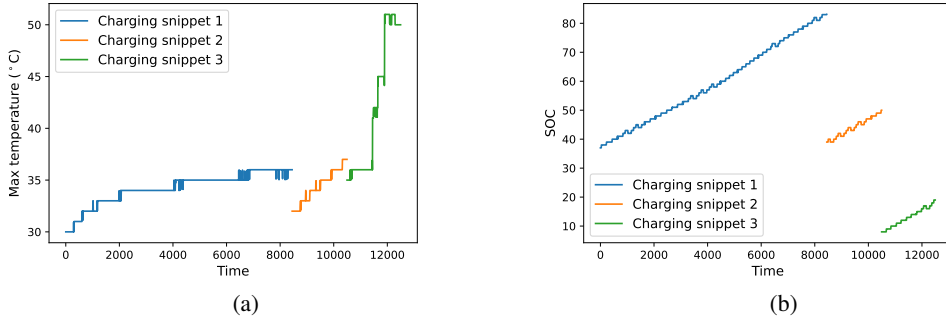


Figure 6: An example of the anomaly in the EV dataset. (a) The max temperature of a vehicle with three charging snippets. (b) The SOC of the battery system with three charging snippets. The third snippet shows a runaway charging temperature, which means that the battery system is already broken.

## B Algorithms implementation details

The ultra implementation details can be found in our released code. We partially use the official and public code resources from PyOD<sup>10</sup>, LSTMAD<sup>11</sup>, GDN<sup>12</sup> and MTAD-GAT<sup>13</sup>. All the experiments are run on a machine with four 2080 Ti GPUs.

### B.1 Autoencoder

The network adopts an encoder-decoder structure with batch normalization layers, drop out layers and sigmoid activation functions. It is built with several fully connected layers. The latent dimensions are [64, 32, 32, 64] in the encoder and decoder. We train the network 20 epochs with a batch size of 128 for the battery dataset, and 5 epoch for the two spacecraft datasets. We use the Adam optimizer with a learning rate of 0.001.

### B.2 Deep SVDD

The feature extraction network of the deep SVDD is an autoencoder with hidden dimensions [64, 32, 32, 64], which is similar to the autoencoder above. The SVDD loss is computed on the middle 32-dimensional latent feature. We also adopt the reconstruction loss to help the network learn better data representation. We train 10 epochs with a batch size of 64 using the Adam optimizer with a learning rate of 0.001 for both the battery dataset and the spacecraft datasets.

### B.3 LSTMAD

The LSTMAD uses the LSTM layers and LSTM cells to encode and decode the input data, respectively. The latent feature dimension is 32. We use an Adam optimizer with a learning rate of 0.001 and train 20 epochs with a batch size of 128 on both the battery dataset and the spacecraft datasets. For the two spacecraft datasets, the window length is set to 128. The reconstruction loss function is the mean absolute error.

### B.4 MTAD-GAT

For the spacecraft dataset, the detection results are directly from the official paper [39]. For the battery dataset, we set the window length to 100 and train the graph network 30 epochs with a batch size of 256. Only the feature dimension number is modified. The other parameters are set to the default value.

### B.5 GDN

We adapt the graph layers to fit our input data. Stacked fully-connected layers are attached at the end of the graph layer. The latent dimension is 128. The window length of the time series data is set to 32 for the battery dataset and 128 for the spacecraft datasets. We use an Adam optimizer with a learning rate of 0.001 to train 20 epochs with a batch size of 128.

### B.6 DyAD

For the battery dataset, we use GRU as the recurrent unit and train the network 3 epochs with a cosine annealing Adam optimizer. The hidden size and latent size are set to 64 and 32, respectively. The spacecraft dataset is pre-processed following [39]. Different snippets are concatenated together. To deal with this special data structure, we use LSTM as the recurrent cell and add a convolutional layer to the decoder. A delayed signal of the encoder is passed to the decoder to compensate for sparse command channels. We train the MSL dataset for 10 epochs and the SMAP dataset for 5 epochs. Both with a cosine annealing Adam optimizer.

---

<sup>10</sup><https://github.com/yzhao062/pyod>

<sup>11</sup><https://github.com/PyLink88/Recurrent-Autoencoder>

<sup>12</sup><https://github.com/d-ailin/GDN>

<sup>13</sup><https://github.com/ML4ITS/mtad-gat-pytorch>

The SWaT dataset provides an official document interpreting each dimension of the data, including the type (sensor or actuator) and a brief description for each dimension. We treat the sensor dimensions as system input and the actuator dimension as system response. We directly apply DyAD on SWaT with a window size of 128.

We notice that another water treatment dataset, WADI [2], is also used in recent works [6]. However, as shown on the official dataset website, the current version of WADI has 127 dimensions, while the reported number of dimensions is 112 in recent research works [6]. Because of the version mismatch, we do not consider using WADI in our experiments.